

Studies on heavy ion fusion and high energy density physics in Japan

S. Kawata^{a,*}, K. Horioka^b, M. Murakami^c, Y. Oguri^b, J. Hasegawa^b, K. Takayama^d,
H. Yoneda^e, K. Miyazawa^a, T. Someya^a, A.I. Ogoyski^{a,f}, M. Seino^a, T. Kikuchi^a,
T. Kawamura^b, M. Ogawa^b

^aUtsunomiya University, Utsunomiya 321-8585, Japan

^bTokyo Institute of Technology, Yokohama 226-8502, Japan

^cOsaka University, Osaka 565-0871, Japan

^dKEK, High Energy Accelerator Research Organization, Tsukuba 305-0801, Japan

^eUniversity of Electro Communications, Chofu 182-8585, Japan

^fVarna Technical University, Varna 9010, Bulgaria

Available online 7 February 2007

Abstract

In this paper, significant progresses of Japanese research activities are presented in heavy ion fusion (HIF) and high energy density physics (HEDP). Heavy ion beam (HIB) is a prominent tool to study HEDP and HIF, and HIBs may be a promising inertial fusion driver. HIB accelerators have been studied intensively for a long time; HIB pulse profile, a particle energy and a HIB quality are controllable. A HIB energy deposition profile is also well defined, and HIB energy is deposited inside a material. By focusing and using the HIB excellent properties, Japanese HIF and HEDP activities have covered a wide variety of subjects ranging from new accelerators to future HIF studies: ion source, new inductive accelerator, beam physics, beam bunching, beam instabilities, HIB interactions with gas or materials, laser ion acceleration, HIB transport, HIB-based warm dense (WD) state generation, new measurement of HED or WD matters, HIB stopping power, atomic physics, multi-HIBs illumination on a target, HIF target implosion, impact ignition scheme, HIB-radiation conversion, radiation confinement and transport in HED matter or in HIF, and so on.

© 2007 Elsevier B.V. All rights reserved.

PACS: 52.58.Hm; 41.75.Ak; 29.27.-a; 52.40.Mj

Keywords: Heavy ion beam; Warm dense matter; High energy density physics; Inertial fusion

1. Introduction

Heavy ion beam (HIB) is a prominent tool to study high energy density physics (HEDP) and heavy ion fusion (HIF), and HIBs may be also a promising inertial fusion driver [1–33]. HIB accelerators have been studied intensively for a long time; HIB pulse profile, particle energy and HIB quality are controllable. HIB energy deposition profile is well defined, and HIB energy is deposited inside a material.

Significant progresses of Japanese research activities are presented in HIF and HEDP. By focusing and using the HIB excellent properties, Japanese HIF and HEDP activities have covered a wide variety of subjects ranging

from new accelerators to future HIF studies: laser-initiated ion source, new inductive accelerator, beam physics, beam bunching, beam instabilities, HIB interactions with gas or materials, laser ion acceleration, HIB transport, HIB-based warm dense (WD) state generation, new measurement of HED or WD matters (WDM), HIB stopping power, atomic physics, multi-HIBs illumination on a target, HIF target implosion, impact ignition scheme, HIB-radiation conversion, radiation confinement and transport in HED matter or in HIF, and so on [7–33].

A new scheme for repetitive and controllable induction devices was proposed to overcome conventional accelerators [8–12]. A proof-of-principle experiment on the accelerator has been completed recently, and this concept should enable us to make study on physics issues of intense charged particle beams.

*Corresponding author. Tel.: +81 28 689 6080; fax: +81 28 689 6009.

E-mail address: kwt@cc.utsunomiya-u.ac.jp (S. Kawata).

In the HIB final transport, several transport schemes have been proposed: preformed channel transport, neutralized ballistic transport (NBT) using a preformed plasma or using a tube liner, ballistic transport in near vacuum, and so on. One of promising transport schemes is NBT, in which preformed-plasma electrons or wall-emitted electrons neutralize the HIB space charge. An ambipolar-field HIB divergence mechanism was discussed [30].

A detail HIB illumination code is coupled with a fluid implosion code to simulate an implosion of a direct-driven pellet, which has a low-density foam layer in the HIB energy deposition layer. The foam layer confines radiation energy and has a role to smooth the HIB non-uniformity. The simulation results shows that a direct-drive target becomes robust against the pellet displacement dz from a reactor chamber center, when the target has a low-density foam layer, in which the radiation energy is confined.

HIB-based HEDP and WDM studies have also served interesting experimental and simulation studies: a coupled plasma experiments, HIB stopping power measurement in a WDM and Rayleigh–Taylor (R–T) instability control.

2. Accelerator physics

2.1. Ion source

Extraction of high-current ion beams from a laser ion source was tested by using a pulsed multi-aperture spherical diode driven by an induction cavity [7]. The source plasma was produced by irradiating a solid Cu block with a Nd–YAG laser (532 nm, 7 ns, 50 mJ). The amplitude and the duration of the extraction voltage were 130 kV and 450 ns, respectively. Beam divergence due to the strong space-charge force during the extraction was suppressed by the focusing action of the spherical geometry. Fluctuation of the extracted beam flux due to the plasma pre-filled in the gap has been eliminated by applying a bias voltage to the control grid on the anode holes. Using this extraction scheme, we obtained a rectangular beam pulse with a rise time as short as $\approx 0.1 \mu\text{s}$. For Cu^+ ions, however, the beam current behind the cathode was limited to $\approx 0.1 \text{ A}$, owing to space-charge effects, as well as to poor geometrical transmission through the cathode sphere. The beam profile and emittance measured behind the cathode were well reproduced by numerical calculations (Fig. 1) using a 3D particle code. We observed no serious deterioration of the beam emittance due to the grid-controlled extraction scheme. To meet the requirement for ion sources for HIF drivers, the beam brightness should be increased further by several factors [34].

2.2. Inductive accelerator

In the accelerator scheme based on the induction modulators, the acceleration and the longitudinal confinement of charged particles are independently achieved with

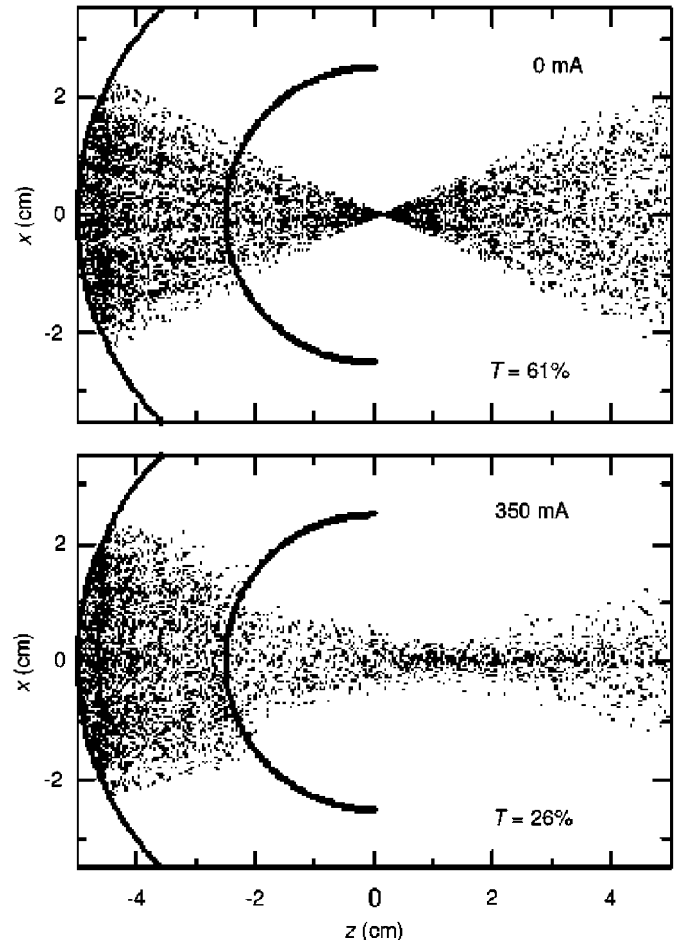


Fig. 1. Calculated beam trajectories behind the source anode for different initial beam currents. The beam transmission through the gap is denoted by T .

controlled step voltages formed by the induction modulators [8–12].

Repetitive and controllable induction modules were developed, including the investigation of magnetic core [8,9,35]. A single bunch acceleration using an induction synchrotron has been demonstrated in KEK [10]. Fig. 2 shows the induction module unit embedded in the KEK proton synchrotron (KEK-PS). A novel method for the transition-energy crossing by using the induction accelerator technique was also investigated in KEK-PS [12]. The capability of the induction accelerator system, which generates a step-pulse of 2 kV output voltage and 18 A output peak current at 1 MHz with 50% duty, has been demonstrated at KEK. The proton bunch could be accelerated from 500 MeV up to 6 GeV with the induction-accelerating device in KEK-PS.

The property of the induction modulators brings us a significant freedom of beam handling, and greatly extends the available longitudinal phase space of charged particles. Based on the inductive modulation scheme, we are planning a variety of studies, such as the beam modulation, beam bunching, momentum selection, and also beam-induced WDM physics.

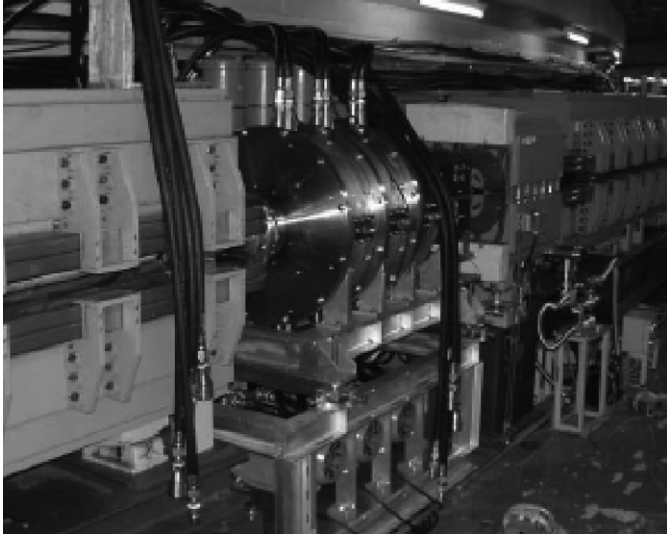


Fig. 2. Inductive accelerator cavity.

3. HIB transport

3.1. Beam bunching

To increase the beam power, the beam bunch should be longitudinally compressed during the transport line in the particle accelerator [36–38]. The beam bunch has the transition from emittance dominated state to space charge dominated one. The emittance growth induced by the space-charge effect due to the longitudinal bunch compression should be studied in the beam physics study. The emittance growth influences the design of the final transport line and the target. The emittance growth and beam instability excited by the space-charge effect were investigated by using an analytical and numerical approaches [13,14]. Also, the effect of dipole oscillations during the longitudinal bunch compression indicates the additional emittance growth. Fig. 3 shows the emittance growth during the final beam bunching with the initial off-centered beam. The multiparticle simulations indicate that the additional emittance growth of about 10% is induced by the dipole oscillation due to the off-centered displacement. The error of the external confinement field in the transport line affects the emittance growth. The transverse field error generates the halo particles, and causes the emittance growth coupled with the space-charge effect.

3.2. Final beam transport

In HIF, HIBs should be transported through a reactor gas in 3–5 m and focused onto a fuel pellet of \sim mm radius. Due to the HIB high current, the HIB space charge should be neutralized in a reactor. We discuss the final transport in a neutralized ballistic final beam transport scheme, and show a HIB divergence by an ambipolar (plasma sheath) field [30] generated by neutralizing electrons.

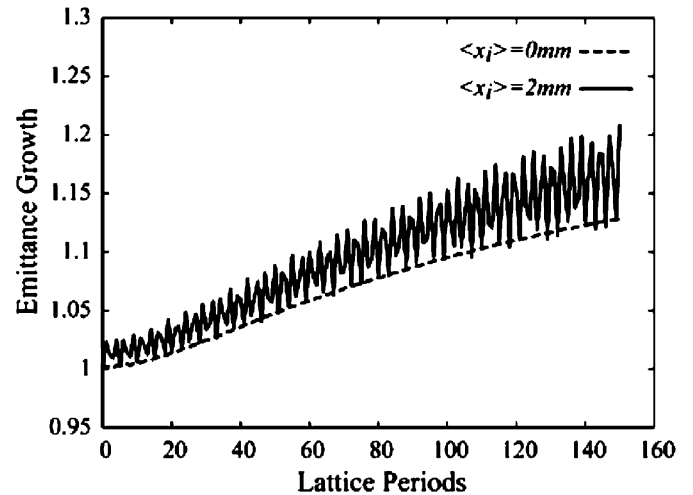


Fig. 3. Emittance growth during the final beam bunching with and without the initial off-centered displacement.

On the other hand, the HIB ion number density increases from $N_{b0} \sim 10^{11} \sim 10^{12} / \text{cm}^3$ at a beam port entrance to $100\text{--}200 \times N_{b0}$ at the fuel pellet position. During the HIB transport, the HIB radius changes from $\sim 2\text{--}3 \text{ cm}$ to $\sim 2\text{--}3 \text{ mm}$. A chamber gas or attached electrons neutralize the HIB space charge well at the beginning transport section of $\sim 1 \text{ m}$ near the reactor wall. Near the fuel pellet at the chamber center, the HIB number density and the neutralizing electron number density increase, and we can also expect the chamber gas photoionization to increase the chamber gas electrons near the target.

When a core plasma is surrounded by a lower density plasma or vacuum and at the same time the core plasma electron has a high temperature, the core plasma expands with a higher speed than the plasma ion thermal speed: high-temperature electrons move out of and back to the core plasma ions and induce a charge separation at the core plasma ion surface. The charge separation extracts the plasma ions and consequently the core plasma expands fast by the ambipolar (plasma sheath) field. In the HIB transport, the HIB ions are the core plasma ions, and the neutralizing electrons may have a high temperature during the HIB convergence. Hereafter, we discuss the HIB divergence by the ambipolar field generated by neutralizing electrons, propose possible solutions to suppress the HIB divergence and present a transport window.

Indirect-driven and direct-driven fuel pellets require several MJ of HIB driver energy in HIF. Each HIB carries $\sim 1\text{--}5 \text{ kA}$ and a HIB ion particle energy may be $\sim 4\text{--}10 \text{ GeV}$, depending on the HIB ion species. At the beam port entrance at a reactor wall, a Pb^+ HIB radius r_{b0} may be $2\text{--}3 \text{ cm}$ and its number density is $N_{b0} \sim 10^{12} / \text{cm}^3$ at a beam port entrance. The Pb^+ HIB radius decreases to $r_b \sim 2\text{--}3 \text{ mm}$ in its radius at the target surface and its number density increases to $N_{bf} \sim 100\text{--}200 \times N_{b0} = 1\text{--}2 \times 10^{14} / \text{cm}^3$ at the fuel pellet position. We focus on a NBT scheme. In this scheme, a chamber gas pressure may be a

few mTorr and a chamber neutral gas density may be $\sim 10^{14}/\text{cm}^3$. The chamber gas electron number density may be $\sim 10^{12}/\text{cm}^{-3}$. In the NBT scheme, electrons are supplied from a preformed plasma or a plasma at a wall, and move together with a HIB to neutralize the HIB space charge. Along with a HIB convergence, the co-moving electron density increases to the same order of the HIB density. Near the chamber wall, the co-moving electron temperature T_{e0} is \sim several ten keV, and near the target area the electron temperature increases to a few hundred keV with the decrease in the HIB radius: if we assume an adiabatic increase in the electron temperature T_e , $T_e \sim T_{e0}(r_{b0}/r_b)^{4/3} \sim 22 \times T_{e0}$.

If we have a high number density N_{ce} ($> Z_b N_b$) of chamber electrons surrounding the HIB compared with the HIB ion number density N_b , like a channel transport scheme, the HIB space charge is always well neutralized. At the central 50–100 cm target area surrounding a fuel pellet, photoionized electrons are supplied from the chamber gas, the HIB is also ionized to $Z_b \sim 6$, and one can expect this situation of $N_{ce} > Z_b N_b$. Therefore, it is expected that HIB is neutralized well at the central area.

On the other hand, near the chamber wall area the HIB number density N_{b0} is expected to be comparable to the background chamber gas electron number density. At the same time, the emitted electrons move together and neutralize the HIB space charge well.

However, at the middle area in NBT between the chamber wall area and the target central area, there may be a situation in which $N_{ce} < Z_b N_b$ and the neutralizing electron temperature T_e is high. In this region, a charge separation between the neutralizing electrons and the HIB ions induces a strong radial electric field to expand the HIB radius (see Fig. 4).

In NBT, if the neutralizing electron number density is $N_{be} = Z_b N_b = 10^{14}/\text{cm}^3$, the neutralizing electron temperature is $T_e = 100$ keV and $N_{ce} < Z_b N_b$, the Debye length of the neutralizing electrons is $\lambda_{De} \sim 0.235$ mm ($< r_b$). In the region A (inside HIB) in Fig. 4, we can assume $N_{be} \sim Z_b N_b$; and in the region B, the ambipolar field potential can be estimated by the Poisson equation. For $\lambda_{De} < r_b$ which is normally approved in NBT

$$\varepsilon_{\perp} \propto \sqrt{\frac{Z_b T_e^{3/2}}{N_b r_b}}. \quad (1)$$

Then, we can estimate $\varepsilon_{\perp}/\varepsilon_{\parallel} \sim (3 \sim 100 \text{ keV})/(4 \sim 10 \text{ GeV})$. The key factor for the ambipolar expansion comes from the

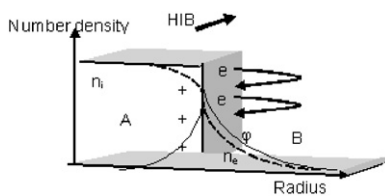


Fig. 4. Neutralizing high-temperature electrons generate a charge separation at a HIB surface. This ambipolar field may expand the HIB in radial.

electron temperature T_e , as is expected. The next important factor is Z_b , that is, a HIB ion charge stripping effect. The possible solutions to suppress the ambipolar field are presented in the following. The ambipolar field supplies a new mechanism or source for HIB divergence, in addition to the effects of the beam space charge, emittance, chromatic aberration and aiming error.

The ambipolar HIB ion divergence phenomenon can be seen in Refs. [39,40], though the ambipolar expansion effect was not recognized in these references. In Refs. [39,40], LSP simulations were performed, and ions located at the HIB outer part in transverse expand seriously. The co-moving electron temperature is also shown in the Ref. [39] and shows a very high temperature of several 10–100 keV.

When a chamber gas electron density N_{ce} is much higher than the HIB number density, that is, $N_{ce} > Z_b N_b$, Eq. (1) also shows a HIB usual neutralization by the background chamber electrons. In this case, normally the chamber electron temperature is low. When $T_e = 10$ eV, $Z_b = 5$, $r_b = 0.4$ cm and $N_{ce} = 10^{14}/\text{cm}^3$, the HIB Pb ions obtain a negligible transverse energy of $\varepsilon_{\perp} \sim 0.05$ keV.

4. HIF studies

4.1. HIF system and pellet gain required

The target energy gain required for energy production by ICF can be evaluated by considering a reactor energy balance. A driver pulse delivers an energy E_d to the target, which releases an amount of fusion energy E_{fus} . The energy gain is $G = E_{fus}/E_d$. The fusion energy is first converted into thermal energy of a blanket in a reactor chamber and then converted into electricity by a standard thermal cycle with an efficiency η_{th} . A fraction f of the electric power is re-circulated to a driver system, which converts it into the HIB energy with an efficiency η_d . The energy balance for this cycle can be written $f\eta_{th}\eta_d G = 1$. Taking $\eta_{th} = 40\%$ and requiring that the recirculated fraction of electrical energy be smaller than $\frac{1}{4}$, we find the condition $G \cdot \eta_d > 10$. For a driver efficiency in the range of $\eta_d = 10 \sim 33\%$, the condition leads to a target gain of $G = 30 \sim 100$ required for power production. Especially, the required pellet gain is about 30 for the HIF, because the HIB driver efficiency is about $\eta_d = 30\%$.

4.2. HIB illumination and fuel pellet implosion

The limited-number-HIB illumination may induce a non-uniform ablation and non-uniform target implosion in realistic cases [41]. In addition, a pellet displacement from the chamber center influences the implosion uniformity and the gain reduction. In order to calculate a fuel target implosion more realistically, we couple a hydrodynamics code with a HIB illumination code [28,29,31] and analyze the target implosion.

In order to study the non-uniformity smoothing effect by the radiation transport in a pellet implosion, we simulate

the target plasma hydrodynamics and fuel ignition by using the hydrodynamics code coupling with the HIB illumination code. Fig. 5(a) shows the fuel target without a foam layer. The Pb, Al and DT layer thicknesses and mass densities are 0.03, 0.40 and 0.10 mm, and 11.3, 2.69 and 0.19 g/cm³, respectively. Fig. 5(b) shows a target with a 0.5 mm thickness foam layer. As widely known, the radiation energy can be confined at a low-density region. The radiation energy confined may smooth the HIB illumination non-uniformity. Therefore, we employ the foam layer to increase the confined radiation energy at the low-density region. The mass density of the foam layer is 0.01 times Al solid density in this study. The HIB pulse consists of a low power (6 TW) part (foot pulse) for the initial 20 ns, a linearly increasing transition phase for 4 ns between 20 and 24 ns, and a high power (320 TW) one (main pulse) for 10 ns. In this case, the total HIB energy is 4.0 MJ. We evaluate the HIB illumination non-uniformity using the RMS (root-mean-square) value. In this section, two-dimensional simulations are performed, and the two-dimensional HIB illumination time-dependent pattern at $\phi = 90^\circ$ is employed from the HIB illumination code [28,29,31].

Fig. 6 shows the mean target density and the mean radiation temperature at (a) 0.29 ns, (b) 40.4 ns and (c) 44.6 ns in the case of the 0.5 mm foam, respectively. Fig. 7 presents (a) the gain curve, (b) the mean ρR and (c) the maximum ion temperature versus dz (the pellet displacement from the reactor chamber center) of the

target displacement for the cases of the radiation transport ON/OFF and without the foam, respectively. As described above, the pellet gain must be larger than 30 in order to get the effective energy production by HIF. In our calculation results, the pellet gain is ~ 23 in the case of $dz = 0$ without the foam. The gain decreases dramatically when the pellet displacement of dz becomes larger in the case without the foam. Therefore, it may be difficult to use a fusion electric power generation system in the case without the foam. On the other hand, we confirm that the pellet gain in the case with the foam is larger than 30 up to dz of about $\sim 300 \mu\text{m}$ pellet displacement. However, the gain becomes smaller with the increase in the pellet displacement dz in the cases of the radiation transport OFF. The mean ρR and the maximum ion temperature in the case of the radiation transport ON are still large compared with those in the cases of the radiation transport OFF and without the foam. From these results, the radiation transport at the low-density foam region plays an important role to release the effective power production by ICF. From our results, the allowable dz in the direct drive mode with a foam in HIF is about $300 \mu\text{m}$. Fig. 8 shows the implosion non-uniformity of (a) the target density and (b) the total pressure at the void closure time as a function of the pellet displacement dz in the cases of the radiation transport ON/OFF and without the foam. These results also indicate that the radiation transport effect at the low-density foam region can relax the non-uniform implosion.

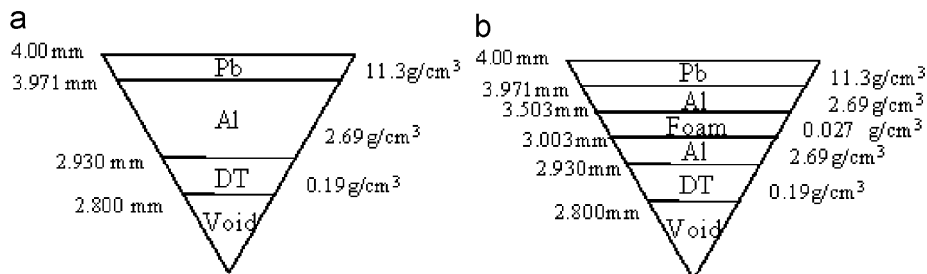


Fig. 5. Target structure of (a) without the foam layer and (b) the 0.5 mm foam.

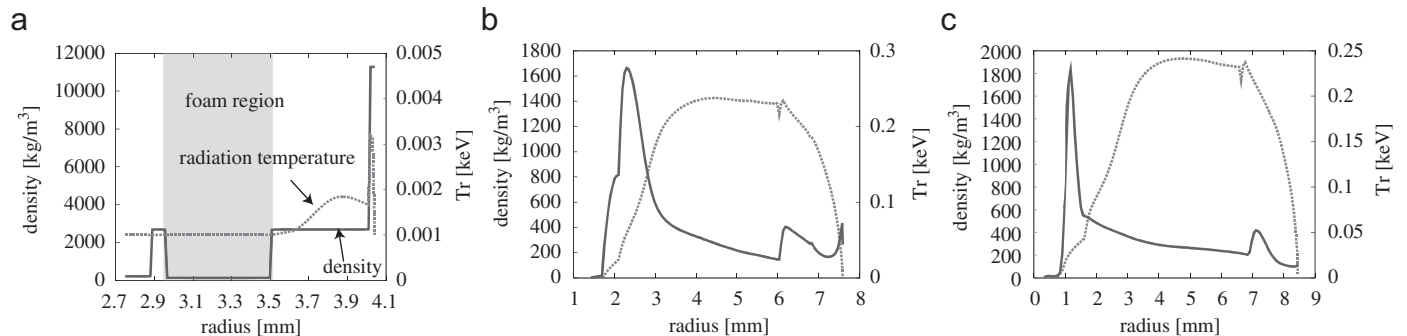


Fig. 6. The mean density and the radiation temperature averaged over the θ direction at (a) 0.29 ns, (b) 40.4 ns and (c) 44.6 ns in the case of the 0.5 mm foam.

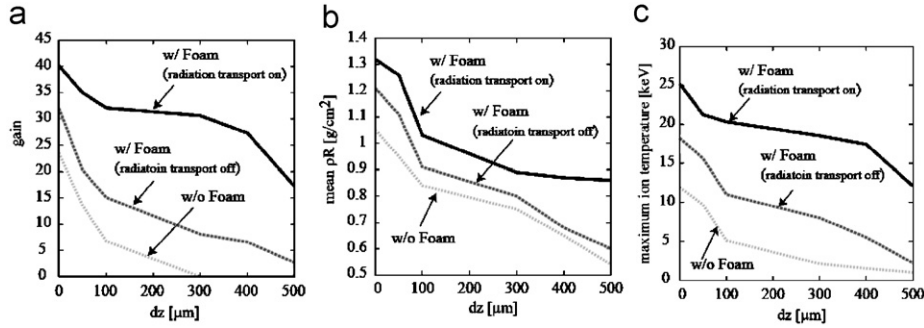


Fig. 7. (a) The pellet gain, (b) the mean ρR and (c) the maximum ion temperature as a function of the pellet displacement dz from the fusion reactor chamber center in the cases of the radiation transport ON or OFF with/without the foam.

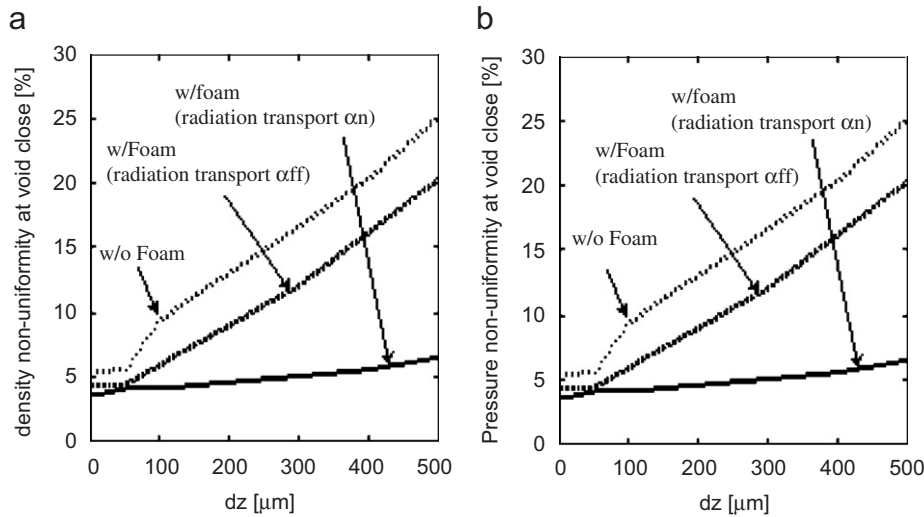


Fig. 8. The implosion non-uniformity of (a) the target density, and (b) the total pressure at the void close time as a function of dz in the cases of the radiation transport ON, OFF and without the foam.

5. HEDP studies

5.1. Merit of HIB

HIB has preferable characteristics for HIF and HEDP studies: (1) controllability of HIB particle energy, HIB direction and HIB pulse length and shape; (2) well-defined energy deposition; and (3) almost classical mechanism of HIB particle energy deposition. These HIB characteristics ensure the viability of HIB as a prominent tool for HEDP and WDM studies, as well as a HIF driver [42,43]. HIB-based WDM and HEDM also have the following interesting features: (1) shock-less heating, (2) volumetric HIB energy deposition, (3) long time scale and (4) high density (for example, $1\text{--}0.1 \times$ solid density). The HIB controllability may also give an interesting possibility of the HIB dynamic control of HIB direction and HIB focusing point. This possibility may open a new method for the R–T instability growth control as shown in Section 5.3.

5.2. WDM experiments

We have comparatively discussed advantages and disadvantages of intense laser facilities, fast pulse power technologies and intense ion beams for HEDP and/or WDM studies. We concluded that ion beams accelerated and modulated using induction modulators could make well-defined WDM over a wide range of parameter regions. Although the possibilities strongly depend on obtainable budget for the facility modification, a research on the beam-target experiments using a modified version of the KEK-PS is planning now [24].

To examine nonlinear ion stopping in warm dense plasma [44,45], a shock-driven plasma target has been developed [46]. An electromagnetic shockwave was driven by a discharge with a peak current of 50 kA in hydrogen gas of 1–5 Torr. Spectroscopic and interferometric measurements determined the density and temperature of the plasma target to be $\sim 5 \times 10^{17} \text{ cm}^{-3}$ and $\sim 1 \text{ eV}$, respectively, which is almost consistent with the prediction from

the measured shock speed (47 km/s). The beam–plasma coupling parameter γ , which is an index parameter for nonlinearity in beam–plasma interaction [47], is given as follows:

$$\gamma = \frac{\sqrt{3}|Z|\Gamma^{3/2}}{(1 + (v^2/v_{\text{th}}^2))^{3/2}}.$$

Here, Z is projectile ion charge, Γ is classical plasma coupling parameter, v is projectile velocity and v_{th} is plasma electron thermal velocity. From the observed plasma parameters, γ is evaluated to be about 0.1 under $v \sim 10$ keV/u and $Z \sim 4$. According to the numerical analysis using a MD simulation [48], nonlinear effects on stopping power are detectable even at $\gamma \sim 0.1$.

A newly designed shock-driven plasma target using a differential pumping system is under development for on-beam experiments. Two 50- μm -diameter orifices suspend a pressure difference between the shock tube and the vacuum beam line, which makes transmittance of ions in the target very small. To detect “single” ion passing through the target and measure its energy, a novel energy-loss-measurement system with a silicon surface barrier detector and a high-speed beam kicker is also tested [25].

Another approach to ion stopping in warm dense plasma is taken by using a thin-foil-discharge (TFD) plasma target [26]. An aluminum or carbon foil target with ~ 0.5 mg/cm² was rapidly heated by a discharge with a peak current of 30 kA. The energy losses of 4.3 MeV/u oxygen and silicon ions in the TFD plasma were observed over phase transition processes of the target from cold solid to warm plasma.

In parallel with the above experimental activities, numerical investigation on low-energy ($v < c/137$) heavy-ion stopping in warm dense plasma was also performed using a Firsov model, in which the projectile energy loss was evaluated from the drag force due to the exchange of electrons between the projectile and the target. A finite-temperature Thomas–Fermi model was applied in order to calculate the spatial and momentum distribution of electrons around the nuclei of the collision partners. We found that the stopping cross-section is more dependent on the density than on the temperature, although the electron distribution around the nuclei changes visibly with the temperature [27].

5.3. R–T instability control by HIB

A linear analysis for the R–T instability under a non-uniform acceleration is studied. The HIB controllability and the well-defined HIB energy deposition may serve the initial well-defined perturbation. Therefore, one may find the initial perturbation amplitude and phase. If we can use a dynamically jiggling HIB and the HIB axis is changed in time, the jiggling HIB may serve a non-uniform acceleration in space and dynamically changing acceleration. As a preliminary study for the R–T instability growth control,

we perform the R–T linear analysis under a spatially non-uniform acceleration [49]. Here, we assume the fluid is incompressible and inviscid. We also assume that the density and the pressure of the zeroth order are the function of the space coordinate z only. First, the non-uniform acceleration is introduced

$$\begin{aligned} g(x, y, z, t) &= g_0 + \delta g(x, y, z, t) \\ &= g_0 + g_1 f_1(x, y) \exp(-\beta|z|) T(t). \end{aligned} \quad (2)$$

In Eq. (2), β is a positive constant, the first order of the acceleration non-uniformity has a spatial dependence of $f(x, y)$ and a time dependence of $T(t)$. The linear analysis for the R–T instability with the first-order acceleration non-uniformity gives the following perturbation of velocity in z :

$$\begin{aligned} w &= \Phi \exp(ik_x x + ik_y y - k|z| + \gamma t) \\ &\quad - g_1 \exp(ik_x x + ik_y y - \beta|z|) t \\ &\equiv w_0 + w_1. \end{aligned}$$

Here, we assume the non-uniform acceleration is in the form of

$$\delta g = g_1 \exp(ik_x x + ik_y y - \beta|z|).$$

Now, we estimate the suppression effect of the non-uniform acceleration field on the R–T instability growth by defining $R = w_0/w_1 \times 100 = g_1 t / \Phi \exp(\gamma t) \times 100$. Here, $\gamma = (gk)^{1/2}$ is the linear growth rate of the R–T instability and k is the instability wave number. At $t = 1$ ns, $R = 23.6, 16.0$ and 11.9 for $k = 10, 50$ and 100 , respectively, at the boundary of the two superposed fluids. In this estimation, the following typical example values are employed: $g_0 = 10^{13}$ m/s², $g_1 = 0.1g_0$ and the initial perturbation amplitude $\Phi = 3.09 \times 10^3$ m/s. This result suggests an interesting realistic scenario for the R–T instability control. First, illuminating HIBs define the initial perturbation amplitude and phase of the non-uniformity introduced. The mode may have the largest perturbation amplitude and should be suppressed. Then, the steerable HIB axes move slightly by a wavelength order to produce g_1 with the inverse phase. In this scenario, the R–T instability growth rate is not reduced, but the growth itself can be reduced significantly as shown above.

Fig. 9 shows example simulation results in the R–T instability control by a spatially non-uniform acceleration. First, the R–T instability is induced by the acceleration non-uniformity for the first 0.5 ns in this example case. Then, the non-uniformity phase is inverted to suppress the R–T growth till 4 ns. The most dangerous R–T instability growth is well reduced at 4 ns.

In addition to this R–T instability control mechanism, HIB may supply different possibilities to control the R–T instability: (1) HIB focusing point can be also shifted or oscillated forward and backward slightly in each bunch. The shift or oscillation of the focusing point may provide a controllability of the HIB-induced non-uniformity, which may also supply g_1 presented above. (2) The successive HIB

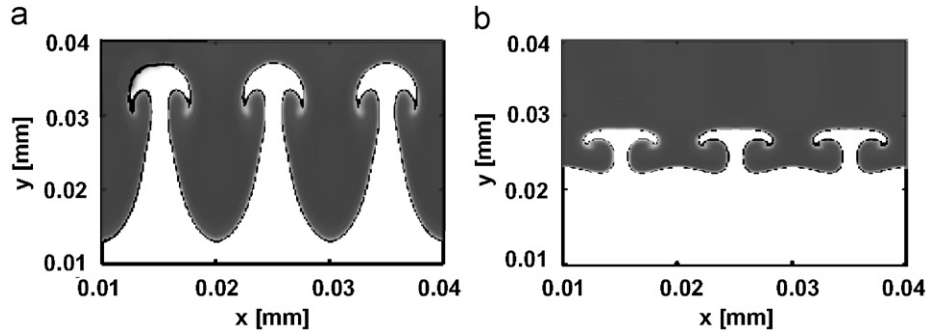


Fig. 9. The Rayleigh–Taylor (R–T) instability control by the spatially non-uniform acceleration: (a) the usual R–T instability induced by the acceleration non-uniformity. (b) The R–T instability growth is well reduced by the phase inversion of the non-uniform acceleration.

short bunches also provides an oscillating acceleration in time. This acceleration dynamic oscillation may also serve a reduction mechanism of the R–T instability in HIB-based WDM or HIF.

6. Conclusions

The significant research progresses in Japanese HIF and HEDP research group are presented in this paper. HIB has preferable features to create a HED or WDM state because HIB deposits its energy inside a material and the pressure gradient in the warm area is less steep. Therefore, the WDM or HEDM region can be confined for a longer time, and this feature may lead the more accurate measurement for various matter states: HIB has opened a new scientific area in the HED and WDM physics. In the accelerator physics, the capability of the KEK induction synchrotron accelerator was demonstrated. In the WDM and HED physics, this paper presented stopping power experiments and the R–T instability control study conducted in Japan. In HIF studies, present research results demonstrated that HIBs provide a promising driver: a rather uniform beam illumination can be realized, and when a low-density foam layer is employed, a robust fuel pellet implosion can be realized against the pellet displacement in a fusion reactor chamber in a direct-driven scheme.

Acknowledgments

This work is partly supported by Japan Society for the Promotion of Science (JSPS) and Ministry of Education, Culture, Sports, Science and Technology (MEXT). The authors would like to present our thanks to all the friends in a HIF research group in VNL, USA, our colleagues in a HIF research group in Japan, Prof. K. Mima, Prof. K. Tachibana and Prof. A.B. Blagoev, for their fruitful discussions on this subject.

References

- [1] B.G. Logan, R.O. Bangert, D.A. Callahan, M. Tabak, M. Roth, L.J. Perkins, G. Caporaso, *Fusion Sci. Technol.* 49 (2006) 399.
- [2] B.G. Logan, F. Bieniosek, C. Celata, et al., *Nucl. Instr. and Meth. A* 544 (2005) 1.
- [3] L.R. Prost, P.A. Seidl, F.M. Bieniosek, et al., *Phys. Rev. ST Accel. Beams* 8 (2005) 020101.
- [4] N.A. Tahir, A. Shutov, I.V. Lomonosov, et al., *High Energy Density Phys.* 2 (2006) 21.
- [5] N.A. Tahir, C. Deutsch, V.E. Fortov, et al., *Phys. Rev. Lett.* 95 (2005) 035001.
- [6] S. Medin, M. Basko, M. Churazov, et al., *Nucl. Instr. and Meth. A* 544 (2005) 300.
- [7] Y. Oguri, K. Kashiwagi, J. Kaneko, J. Hasegawa, M. Yoshida, M. Ogawa, *Phys. Rev. ST Accel. Beams* 8 (2005) 060401.
- [8] M. Watanabe, M. Nakajima, K. Horioka, *Nucl. Instr. and Meth. A* 464 (2001) 440.
- [9] K. Horioka, M. Nakajima, M. Watanabe, et al., *Laser Part. Beams* 20 (2002) 609.
- [10] K. Takayama, K. Koseki, K. Torikai, et al., *Phys. Rev. Lett.* 94 (2005) 144801.
- [11] Y. Shimosaki, E. Nakamura, K. Takayama, K. Torikai, M. Watanabe, M. Nakajima, K. Horioka, *Phys. Rev. ST Accel. Beams* 7 (2004) 014201.
- [12] Y. Shimosaki, K. Takayama, K. Torikai, *Phys. Rev. Lett.* 96 (2006) 134801.
- [13] T. Kikuchi, M. Nakajima, K. Horioka, T. Katayama, *Phys. Rev. ST Accel. Beams* 7 (2004) 034201.
- [14] T. Kikuchi, T. Someya, S. Kawata, et al., *Nucl. Instr. and Meth. A* 558 (2006) 122.
- [15] Y. Oguri, K. Tsubuku, A. Sakumi, K. Shibata, R. Sato, K. Nishigori, J. Hasegawa, M. Ogawa, *Nucl. Instr. and Meth. B* 161–163 (2000) 155.
- [16] A. Sakumi, K. Shibata, R. Sato, K. Tsubuku, T. Nishimoto, J. Hasegawa, M. Ogawa, Y. Oguri, T. Katayama, *Nucl. Instr. and Meth. A* 464 (2001) 231.
- [17] M. Kojima, M. Mitomo, T. Sasaki, J. Hasegawa, M. Ogawa, *Laser Part. Beams* 20 (2002) 475.
- [18] K. Shibata, K. Tsubuku, T. Nishimoto, J. Hasegawa, M. Ogawa, Y. Oguri, A. Sakumi, *J. Appl. Phys.* 91 (2002) 4833.
- [19] J. Hasegawa, N. Yokoya, Y. Kobayashi, M. Yoshida, M. Kojima, T. Sasaki, H. Fukuda, M. Ogawa, Y. Oguri, T. Murakami, *Laser Part. Beams* 21 (2003) 7.
- [20] K. Horioka, M. Nakajima, T. Sasaki, T. Mizoguchi, *Proceedings of the 15th International Conference on High Power Particle Beams, St-Petersburg, D.V. Efremov Institute, Russia, 2004*, pp. 894–897.
- [21] H. Yoneda, H. Morikami, K. Ueda, R.M. More, *Phys. Rev. Lett.* 91 (2003) 075004.
- [22] T. Sasaki, Y. Yano, M. Nakajima, T. Kawamura, K. Horioka, *Laser Part. Beams* 24 (2006) 1.
- [23] K. Kondo, M. Nakajima, T. Kawamura, K. Horioka, *Rev. Sci. Instrum.* 77 (2006) 036104.
- [24] K. Horioka, et al., *High energy density physics researches based on induction accelerator and pulse power technology*, in: *Proceedings of the Recent Progress in Induction Accelerators (RPIA) 2006*.

- [25] S. Nishinomiya, K. Katagiri, T. Niinou, J. Kaneko, H. Fukuda, J. Hasegawa, Y. Oguri, M. Ogawa, Experimental apparatus for the measurement of non-linear stopping of low-energy heavy ions, to appear in *Nucl. Instr. and Meth. A*, (2007), doi:10.1016/j.nima.2007.02.067.
- [26] J. Hasegawa, K. Katagiri, M. Yonaha, H. Fukuda, Y. Oguri, M. Ogawa, Interaction experiments using thin-foil-discharge warm-dense plasma, to appear in *Nucl. Instr. and Meth. A*, (2007), doi:10.1016/j.nima.2007.02.034.
- [27] Y. Oguri, T. Niinou, S. Nishinomiya, K. Katagiri, J. Kaneko, J. Hasegawa, M. Ogawa, Firsov approach to the heavy-ion stopping in warm matter using a finite-temperature Thomas–Fermi model, to appear in *Nucl. Instr. and Meth. A*, (2007), doi:10.1016/j.nima.2007.02.009.
- [28] A.I. Ogoyski, T. Someya, S. Kawata, *Comput. Phys. Commun.* 157 (2004) 160.
- [29] T. Someya, A.I. Ogoyski, S. Kawata, T. Sasaki, *Phys. Rev. ST Accel. Beams* 7 (2004) 044701.
- [30] S. Kawata, R. Sonobe, T. Someya, T. Kikuchi, *Nucl. Instr. and Meth. A* 544 (2005) 98.
- [31] S. Miyazawa, A.I. Ogoyski, S. Kawata, T. Someya, T. Kikuchi, *Phys. Plasmas* 12 (2005) 122702.
- [32] S. Neff, R. Knobloch, D.H.H. Hoffmann, A. Tauschwitz, S.S. Yu, *Laser Part. Beams* 24 (2006) 71.
- [33] C. Deutsch, G. Maynard, R. Bimbot, D. Gardes, S. Della-Negra, M. Dumail, B. Kubica, A. Richard, M.F. Rivet, A. Servajean, C. Fleurier, A. Sanba, D.H.H. Hoffmann, K. Weyrich, H. Wahl, *Nucl. Instr. and Meth. A* 278 (1989) 38.
- [34] J.W. Kwan, D. Baca, E. Henestroza, et al., *Nucl. Instr. and Meth. A* 544 (2005) 134.
- [35] A.W. Molvik, A. Faltens, *Phys. Rev. ST Accel. Beams* 5 (2002) 080401.
- [36] R.C. Davidson, H. Qin, *Phys. Rev. ST Accel. Beams* 8 (2005) 064201.
- [37] H. Qin, R.C. Davidson, J.J. Barnard, E.P. Lee, *Nucl. Instr. and Meth. A* 544 (2005) 255.
- [38] P.K. Roy, S.S. Yu, E. Henestroza, et al., *Phys. Rev. Lett.* 95 (2005) 234801.
- [39] D.V. Rose, D.R. Welch, B.V. Oliver, R.E. Clark, W.M. Sharp, A. Friedman, *Nucl. Instr. and Meth. A* 464 (2001) 299.
- [40] D.R. Welch, D.V. Rose, B.V. Oliver, R.E. Clark, *Nucl. Instr. and Meth. A* 464 (2001) 134.
- [41] S. Skupsky, K. Lee, *J. Appl. Phys.* 54 (1983) 3662.
- [42] D.H.H. Hoffmann, A. Blazevic, P. Ni, et al., *Laser Part. Beams* 23 (2005) 47.
- [43] N.A. Tahir, A. Adonin, C. Deutsch, et al., *Nucl. Instr. and Meth. A* 544 (2005) 16.
- [44] G. Maynard, K. Katsonis, C. Deutsch, G. Zwicknagel, M. Chabot, D. Gardes, *Nucl. Instr. and Meth. A* 464 (2001) 86.
- [45] G. Maynard, C. Deutsch, K. Dimitriou, K. Katsonis, M. Sarrazin, *Nucl. Instr. and Meth. B* 195 (2002) 188.
- [46] K. Katagiri, S. Nishinomiya, T. Niinou, J. Kaneko, J. Hasegawa, Y. Oguri, Development of a non-ideal plasma target for non-linear beam-plasma interaction experiments, to appear in *Nucl. Instr. and Meth. A*, (2007), doi:10.1016/j.nima.2007.02.066.
- [47] G. Zwicknagel, C. Toepffer, P.-G. Reinhard, *Phys. Rep.* 309 (1999) 117.
- [48] Y. Oguri, J. Hasegawa, J. Kaneko, M. Ogawa, K. Horioka, *Nucl. Instr. and Meth. A* 544 (2005) 76.
- [49] S. Kawata, T. Sato, T. Teramoto, et al., *Laser Part. Beams* 11 (1993) 757.